LMU LUDWIG-MAXIMILIANS-UNIVERSITÄT MÜNCHEN

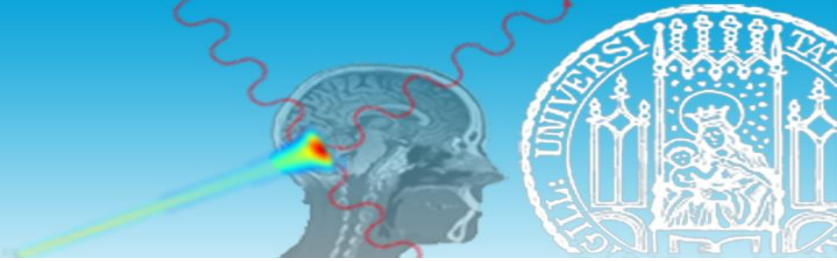

Inverse problems and machine learning in medical physics

Imaging in ion beam therapy

Dr. Chiara Gianoli
29/11/2022
chiara.gianoli@physik.uni-muenchen.de

Radiation oncology

- Radiotherapy is a cancer treatment that makes use of ionizing radiation (photons or ions) to damage the DNA of cancerous tissue, inducing cellular death

- Physical and biological considerations depending on the ionizing radiation

	Ions	Photons
Physics	Better targeting due to the "Bragg peak"	Reduced sensitivity to anatomical uncertainties
Biology	Enhanced radiobiological effectiveness, mostly due to linear energy transfer – density of ionizations	Oxygen enhancement ratio, inhibited by tumor hypoxia

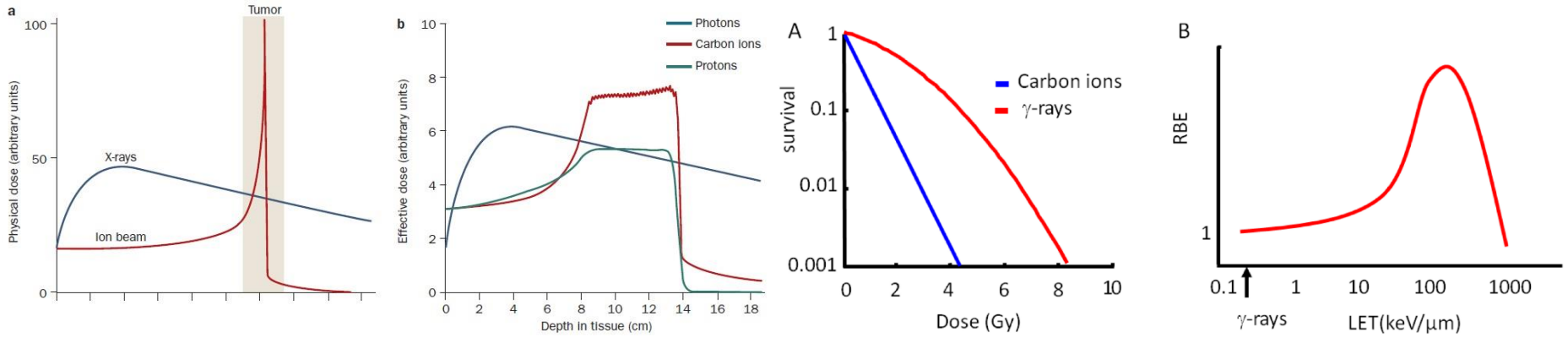

Durante, M., & Loeffler, J. S. (2010). Charged particles in radiation oncology. *Nature reviews Clinical oncology*, 7(1), 37-43.

Ledingham, K. W., Bolton, P. R., Shikazono, N., & Ma, C. M. C. (2014). *Towards laser driven hadron cancer radiotherapy: A review of progress*. Applied Sciences, 4(3), 402-443.

The role of imaging in radiation oncology

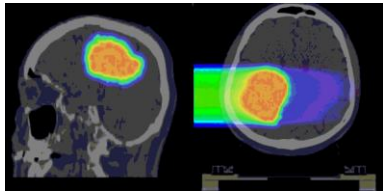

define the geometry

Treatment planning

Treatment adaptation

reproduce the geometry

Treatment delivery

Treatment verification

Off-line

check the geometry

In-room

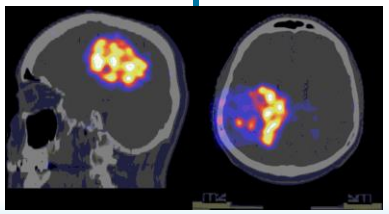

Treatment planning

- The anatomical identification of the target is typically based on X-ray imaging, or X-ray Computed Tomography (CT)
  - The X-ray beam rotates across the patient
  - The density of the tissue attenuates the X-ray beam intensity
- The functional information based on Positron Emission Tomography (PET) can complement the target identification, based on molecular uptake and metabolism
  - The radiotracer is administered in the patient
  - The β^+ emitters concentrate in the tumor due to biological properties of the radiotracer

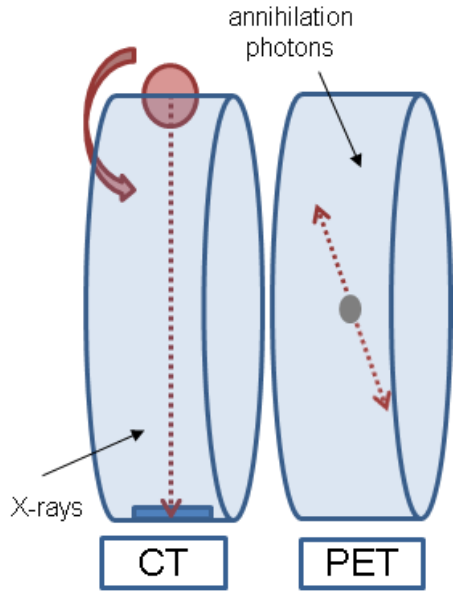

Treatment planning

- Multi-modality imaging is used to construct a model of the patient in the treatment planning scenario
  - X-ray CT is the primary anatomical image for treatment planning
  - PET as secondary images for the delineation of the functional tumor
  - Magnetic resonance imaging (MRI) as secondary anatomical and functional image (i.e., soft tissue delineation and tumor microstructure)

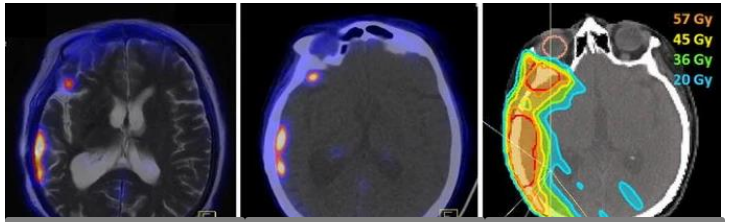

Thorwarth, D., Leibfarth, S., & Mönnich, D. (2013). Potential role of PET/MRI in radiotherapy treatment planning. *Clinical and Translational Imaging*, 1(1), 45-51.

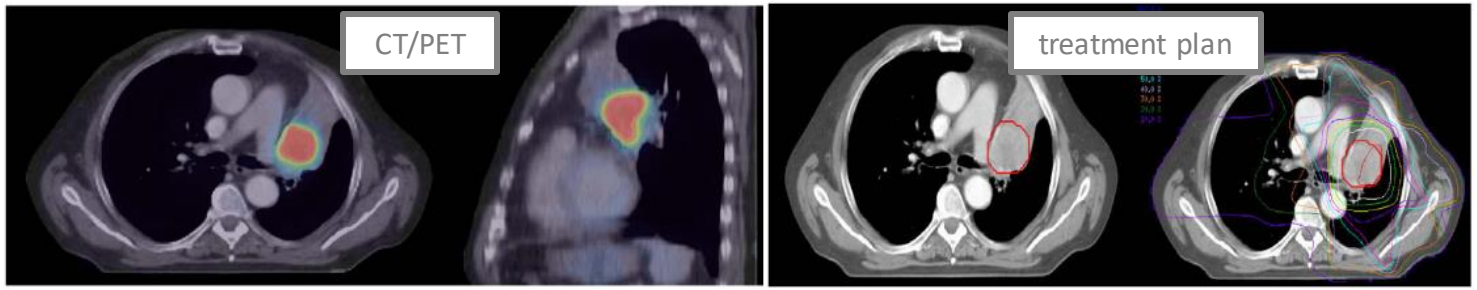

MacManus, M., Nestle, U., Rosenzweig, K. E., Carrio, I., Messa, C., Belohlavek, O., ... & Jeremic, B. (2009). Use of PET and PET/CT for radiation therapy planning: IAEA expert report 2006–2007. *Radiotherapy and oncology*, 91(1), 85-94.

Treatment delivery

- The in-room patient anatomy (i.e., the treatment delivery scenario) is matched to the model of the patient anatomy (i.e., the treatment planning scenario)

- Lying on the treatment couch, the patient is rigidly aligned to the treatment planning scenario prior to treatment delivery

  - In-room optical systems

  - In-room X-ray imaging systems

    - "mega-voltage" electronic portal imaging devices (EPID) in photon therapy

    - "mega-voltage/kilo-voltage" fluoroscopic imaging

    - "kilo-voltage" imaging from auxiliary imaging systems (i.e., cone beam CT)

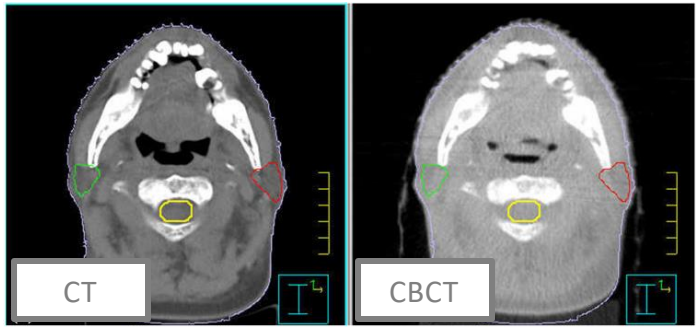

Hu, W., Ye, J., Wang, J., Ma, X., & Zhang, Z. (2010). Use of kilovoltage X-ray volume imaging in patient dose calculation for head-and-neck and partial brain radiation therapy. *Radiation Oncology*, 5(1), 1-10.

Treatment verification

- An *indirect* treatment verification can be performed during or immediately after ion beam therapy

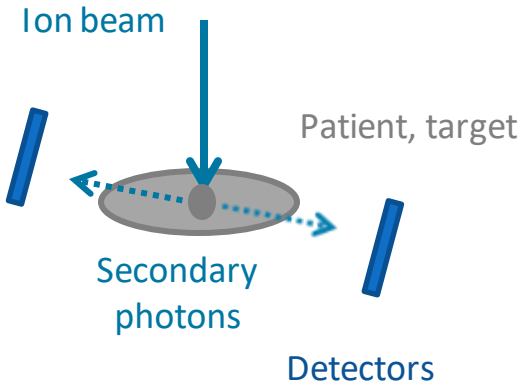

- PET imaging of the annihilation photon pairs relevant to β^+ emitting nuclei produced by nuclear fragmentation
- Prompt-γ photons imaging relevant to nuclear de-excitation

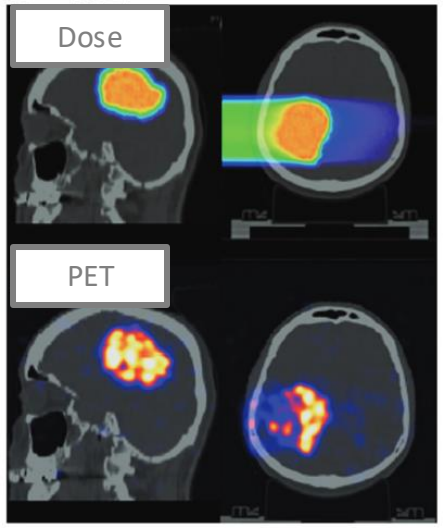

Parodi, K. (2012). PET monitoring of hadrontherapy. *Nuclear Medicine Review*, 15(C), 37-42.

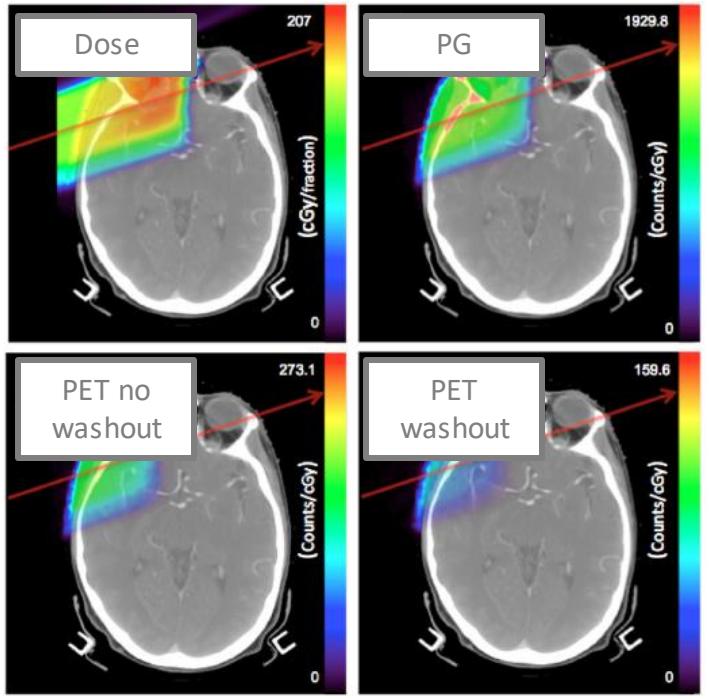

Moteabbed, M., España, S., & Paganetti, H. (2011). Monte Carlo patient study on the comparison of prompt gamma and PET imaging for range verification in proton therapy. *Physics in Medicine & Biology*, 56(4), 1063.

Treatment verification

- PET-based treatment verification in ion beam therapy, immediately after proton therapy

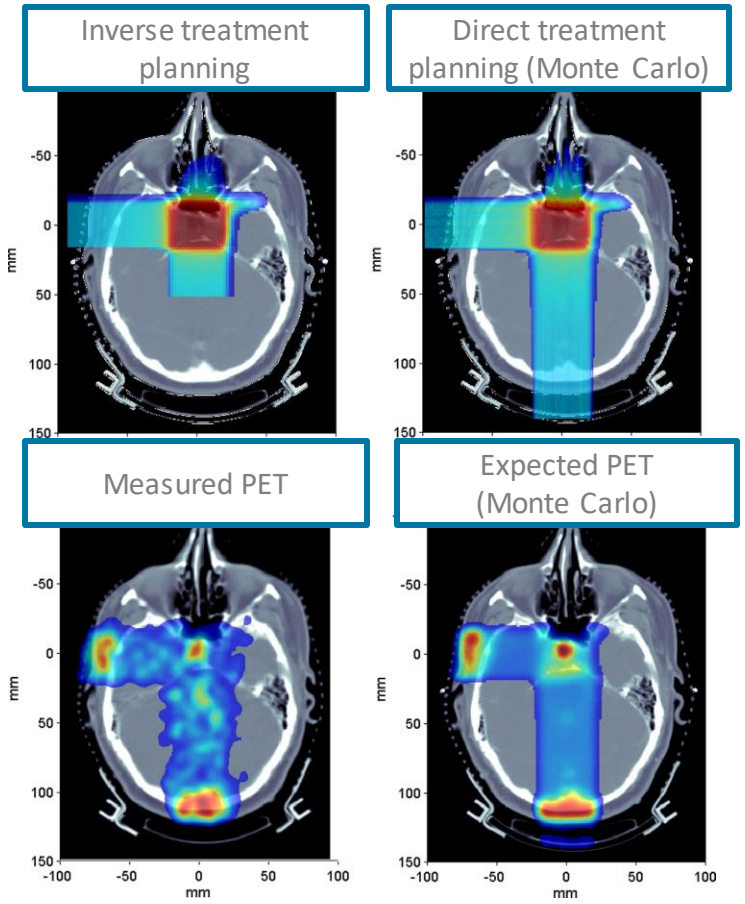

Parodi, K., Paganetti, H., Shih, H. A., Michaud, S., Loeffler, J. S., DeLaney, T. F., ... & Bortfeld, T. (2007). Patient study of in vivo verification of beam delivery and range, using positron emission tomography and computed tomography imaging after proton therapy. International Journal of Radiation Oncology* Biology* Physics, 68(3), 920-934.

Treatment verification

- A *direct* treatment verification (i.e., dosimetry) can be performed during photon beam therapy

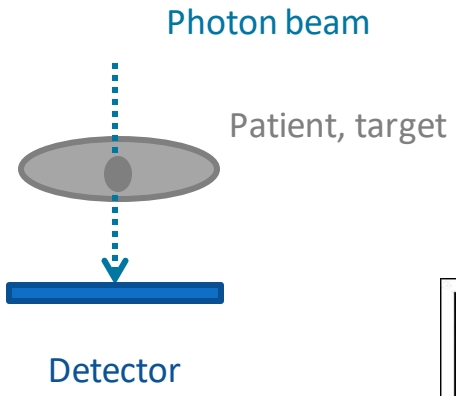

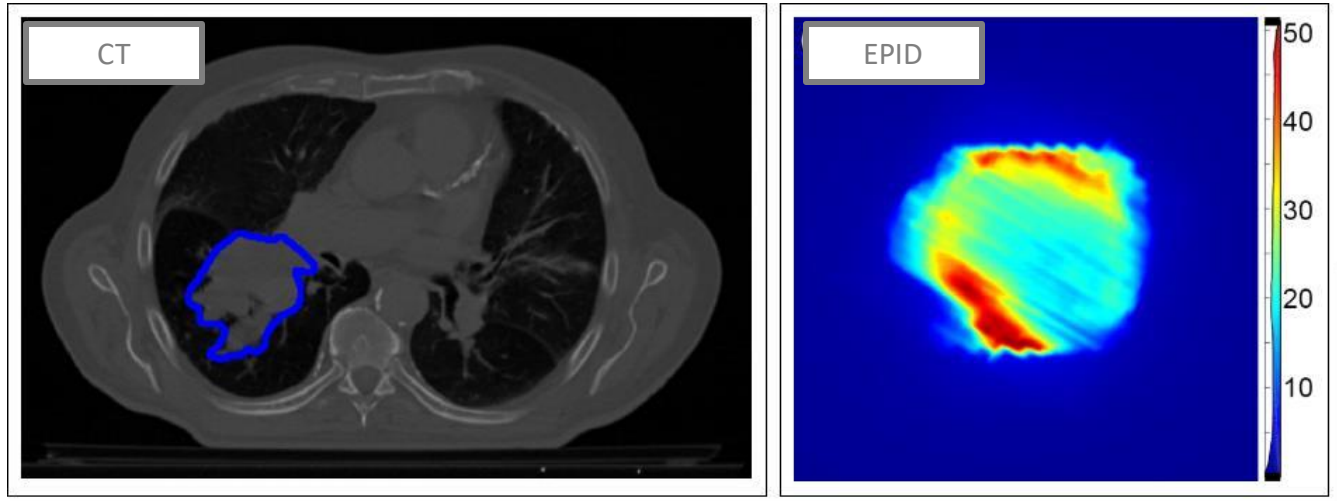

Wolfs, C. J., Canters, R. A., & Verhaegen, F. (2020). Identification of treatment error types for lung cancer patients using convolutional neural networks and EPID dosimetry. *Radiotherapy and Oncology*, 153, 243-249.

Treatment adaptation

- The patient model is updated and the treatment is re-planned
  - Deformable image registration of the treatment planning CT (moving image) to the “CT of the day” (fixed image)
  - Contour propagation (i.e., application of the resulting deformation field) for the segmented anatomical structures (recontouring is time consuming…)

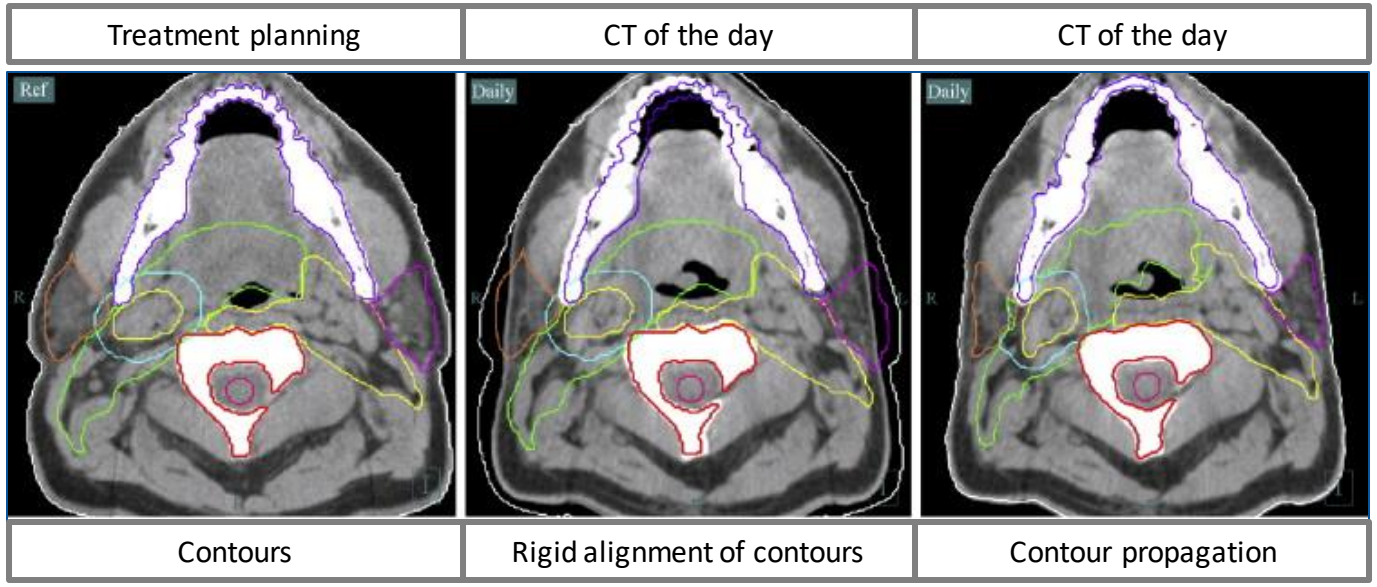

Schwartz, D. L., Garden, A. S., Thomas, J., Chen, Y., Zhang, Y., Lewin, J., … & Dong, L. (2012). Adaptive radiotherapy for head-and-neck cancer: initial clinical outcomes from a prospective trial. *International Journal of Radiation Oncology* Biology* Physics*, 83(3), 986-993.

Ion imaging in treatment planning

- Treatment planning in ion beam therapy is based on X-ray imaging but the native imaging technique for ion beam therapy is ion imaging
  - The X-ray CT image, expressed as Hounsfield Unit (HU), is semi-empirically calibrated into relative stopping power (RSP) to match the physical properties of the therapeutic radiation
  - The calibration curve is defined by piecewise linear fitting of the theoretical HU, parameterized based on experimental HU of tissue equivalent materials with known elemental composition, and theoretical RSP, calculated according to the Bethe-Bloch model (i.e., the "stoichiometric calibration")
    - Uncertainties are associated to elemental composition, mass density and mean ionization energy of real tissue

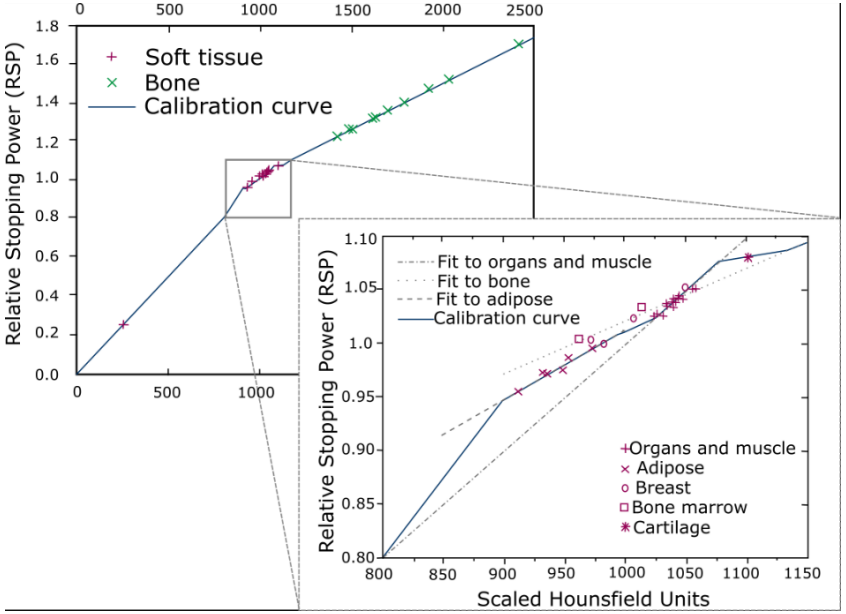

Proton

$$S/\rho \propto \frac{Z}{A}\frac{1}{\beta^2}\left(\ln\left(\frac{2m_e c^2 \beta^2}{I_m (1-\beta^2)}\right) - \beta^2\right)$$

ρ mass density, $\frac{Z}{A}\rho$ electron density, I_m mean ionization energy

Schneider et al. 1996 *Phys. Med. Biol.*

Ion imaging in treatment planning

- Semi-empirical calibration of HU into RSP is associated to inaccuracies in dose calculation and therefore, in treatment planning
  - From 1.1% (soft tissue) to 1.8% (cortical bone)
  - Up to 5% (lung)
- X-ray CT artefacts due to beam hardening (causing inaccuracy in the linear projection model…) are also responsible for inaccuracies in ion range estimation
  - Steel or titanium prosthesis, from 5% to 18% (hip)
  - Gold feelings, up to 3%

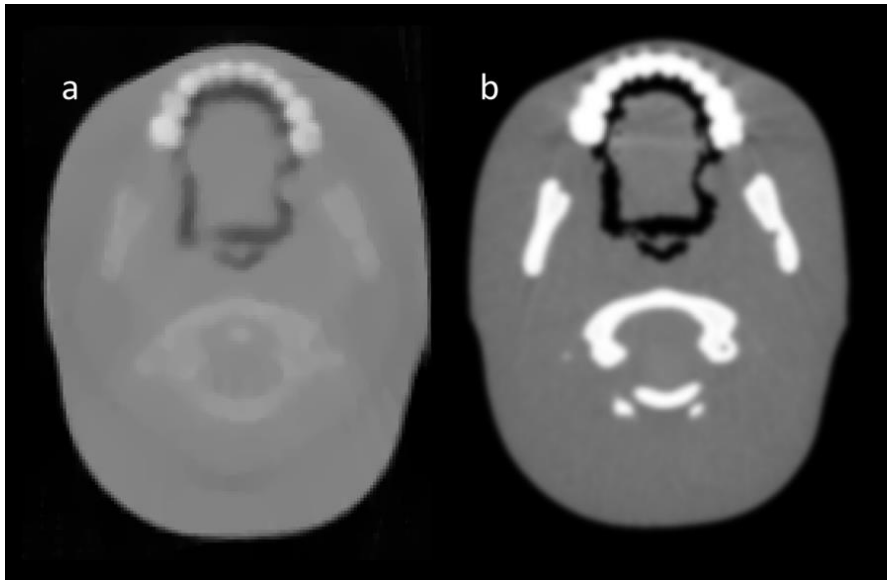

proton CT X-ray CT

Johnson, R. P. (2017). Review of medical radiography and tomography with proton beams. Reports on progress in physics, 81(1), 016701.

Ion imaging

- Ion imaging offers the promise of eliminating these inaccuracies by measuring the water equivalent thickness (WET) of the traversed object of interest
  - The WET (i.e., the ion radiography) is modeled as a line integral of the RSP (i.e., the ion image) along a certain concept of ion trajectory that depends on the detector configuration

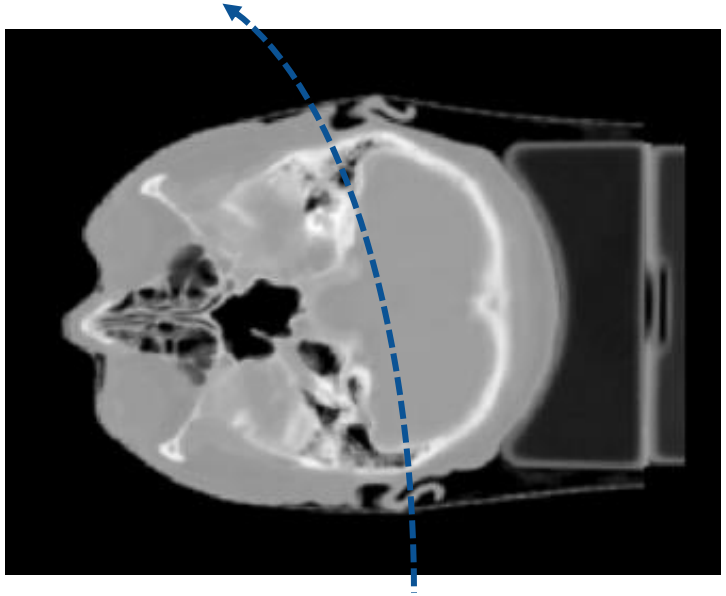

$$WET_i = \sum_j a_{ij} RSP_j$$

- The a_{ij} describes the intersection length/area/volume of the ion trajectory i with each voxel j
- The a_{ij} is the coefficient of the system matrix A that describes the forward-projection model $\overrightarrow{WET} = A * \overrightarrow{RSP}$ as a system of linear equations

Fundamentals of ion imaging

- The forward-projection model depends on the detector configuration

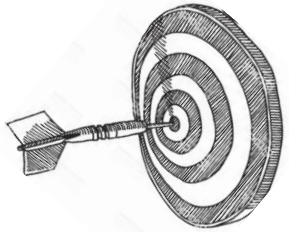

List-mode detector

- The concept of ion trajectory for a single ion is the *ion trajectory*
  - "Spindle" Gaussian uncertainties

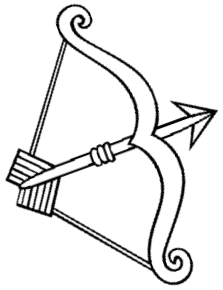

- The concept of ion trajectory for a pencil beam is the *mean ion trajectory*
  - Conical Gaussian uncertainties

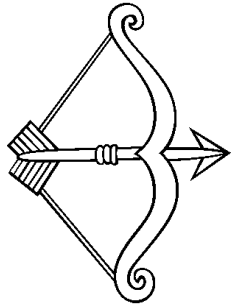

Integration-mode detector

Fundamentals of ion imaging

- Measurement of the *range* of the single ion or the *mean range* of the pencil beam to retrieve the integral inverse stopping power ("stopping power" information)
  - The *mean range* is defined as the integral over energy of the inverse stopping power (initial beam energy known from acceleration setting)

$$\int_{E_i}^{0} \frac{dx}{dE} dE$$

- Measurement of *position* and *angle* of the single ion prior and after the object of interest to retrieve the integral scattering power ("scattering power" information)
  - The scattering model describes these variables as Gaussians, and the *standard deviations of position and angle* are defined as the integral over space of the scattering power

$$\int_0^x \frac{d\sigma_p}{dx} dx, \int_0^x \frac{d\sigma_a}{dx} dx$$

List-mode detector configuration for single ions

- The scattering power of the ion is retrieved from the measurement of the position (or the position and the angle) prior and after the object of interest by means of single (or double) thin tracking layers

- The stopping power of single ions can be retrieved from:
  - Single absorption and detection block measuring the residual energy[1,2]
  - Multiple absorption layers interleaved by detection layers measuring multiple energy losses[3,4]

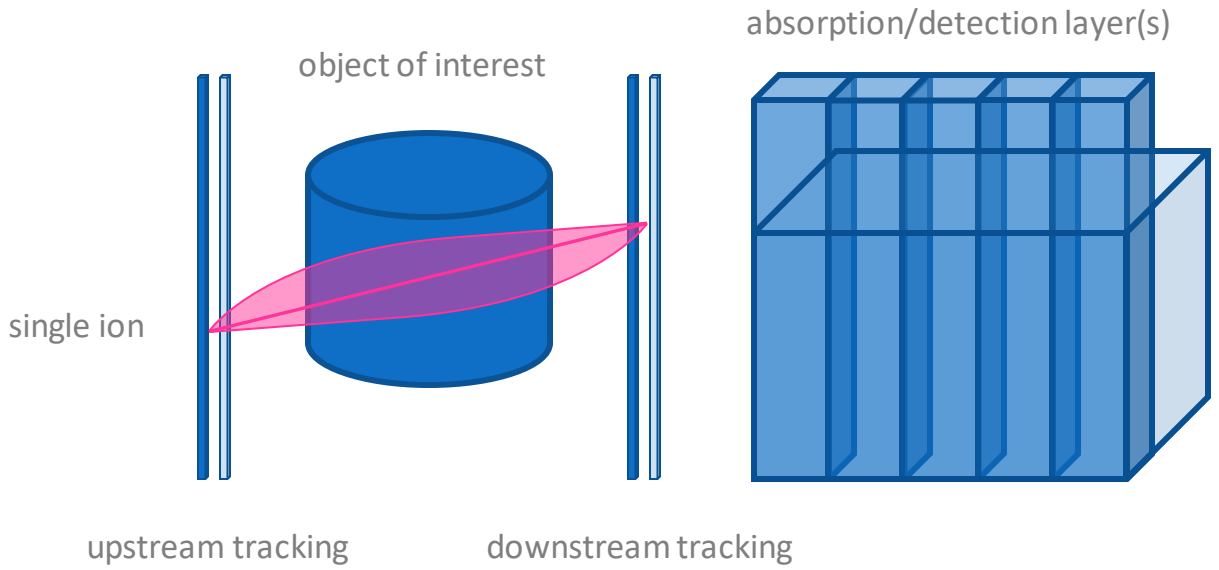

- Fast tracking layers can retrieve the scattering power and the stopping power from the time of flight of the tracked ion (i.e., 4D trackers) after the object of interest[5]

- The energy/range measurement is then converted to WET

[5]Ulrich-Pur et al. 2022 *Phys. Med. Biol.*

Pioneer detector configurations
[1]Schneider and Pedroni 1995 *Med. Phys.*
[2]Sadrozinsky et al. 2004 *IEEE Trans. Nucl. Sci.*
[3]Pelmer et al. 1999 *Nucl. Instrum. Methods Phys. Res. A*
[4]Bashkirov et al. 2016 *Nucl. Instrum. Methods Phys. Res. A*

Integration-mode detector configuration for pencil beams

- The stopping power of single ions can be retrieved from:
  - Single absorption and detection block measuring the residual energy of the pencil beam
    - The mean energy/range is converted to WET
  - Multiple absorption layers interleaved by detection layers measuring multiple energy losses (i.e., the Bragg peak signal)[1] or single absorption and detection layer measuring the energy loss at multiple initial energies of the pencil beam[2,3]
    - The mixed energy/range is statistically resolved and converted to an histogram of WET components and occurrences (the mode WET component or the mean WET component are then selected)
  - Pixelated layers can statistically resolve also the scattering power of the pencil beam

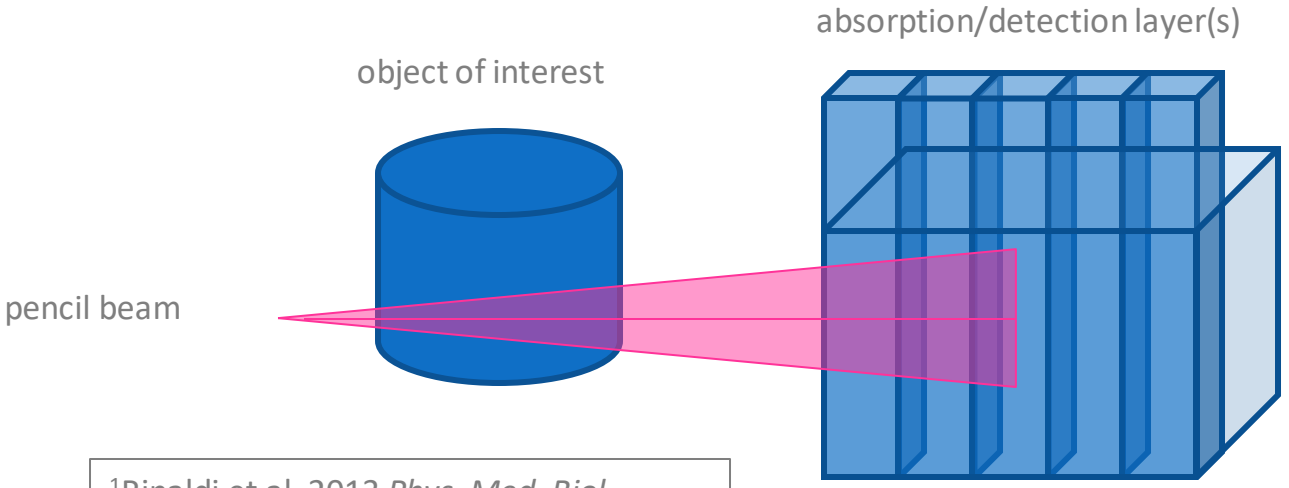

[1]Rinaldi et al. 2013 *Phys. Med. Biol.*
[2]Testa et al. 2013 *Phys. Med. Biol.*
[3]Telsemeyer et al. 2012 *Phys. Med. Biol.*

Integration-mode detector configuration for pencil beams

- In integration-mode detector configuration, the Bragg peak signal for each pencil is discretized according to the multiple layers (i.e., channels) or according to the multiple initial energies in a single layer

- Due to lateral inhomogeneity traversed by the pencil beam, the Bragg peak signal results in a linear combination of elementary Bragg peak signals

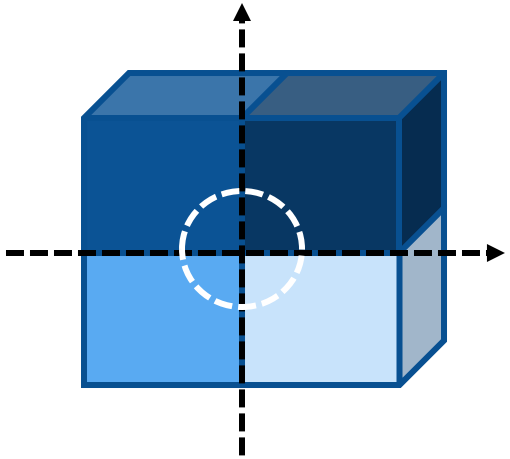

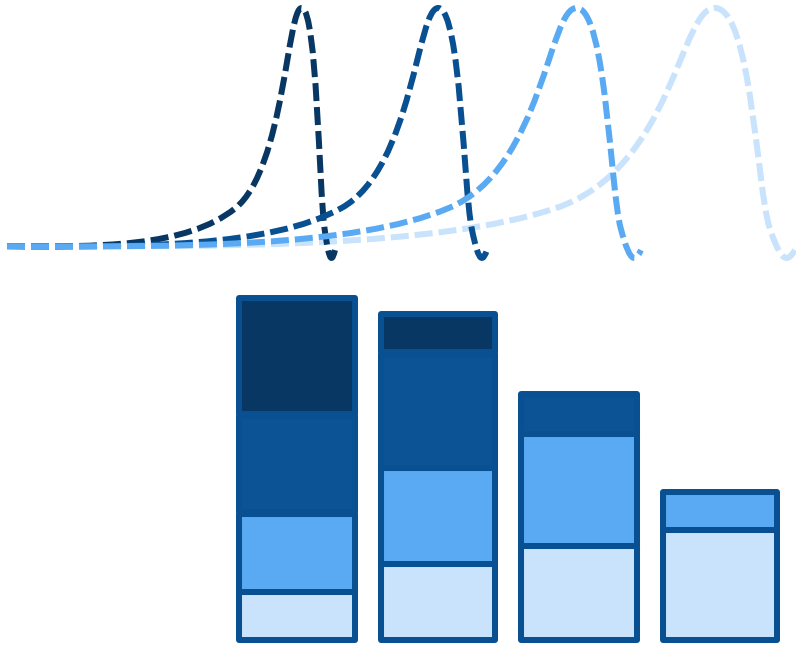

- The Bragg peak of the component with the larger WET (i.e., the shorter range) takes advantages from the Bragg peaks of the components with smaller WET

Integration-mode detector configuration for pencil beams

- Linear decomposition[1,2] (inverse problem) is applied to retrieve the WET histogram as WET occurrence for each WET component by solving the system of linear equations $\overrightarrow{BP} = LUT * \overrightarrow{WET}$
  - $\overrightarrow{BP}$ is the discretized Bragg peak signal
    - $\overrightarrow{WET}$ is the unknown vector of WET occurrences
    - LUT is the look-up-table of individual Bragg peak signals for each WET component
  - The least square optimization is based on Euclidean distance minimization

$$argmin_{\overrightarrow{WET}} \frac{1}{2} \left\| LUT * \overrightarrow{WET} - \overrightarrow{BP} \right\|_2^2$$

  - An histogram of WET occurrences for each WET component is obtained

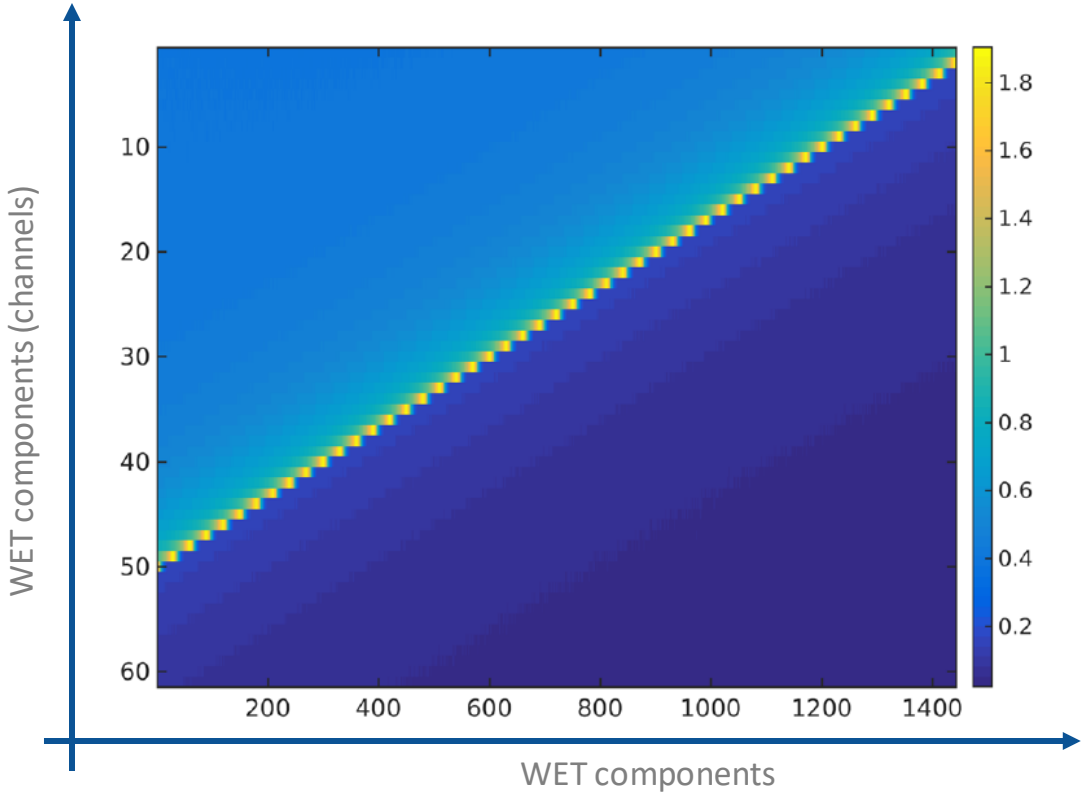

[1]Krah et al. 2015 *Phys. Med. Biol.*
[2]Meyer et al. 2017 *Phys. Med. Biol.*

Detector configuration and ion trajectories

- Due to the stochastic nature of the multiple Coulomb scattering, the ion trajectory of the single ion is known at the entrance and the exit of the object of interest but uncertain in between and thus, modeled according to a "spindle" Gaussian distribution
  - Maximum likely path (MLP) accounts for the scattering power of the single ion in list-mode detector configuration[1]
  - MLP approximation[2] or machine learning[3] can be adopted

- For integration-mode detector configuration, the typical concept of ion trajectory is the mean ion trajectory
  - As the nominal pencil beam dimension and direction are known, the model (in water) or the measurement (if available) of the scattering power corresponds to a flared conical Gaussian distribution for each WET component
- The model in water equivalent materials based on the X-ray CT image can be considered

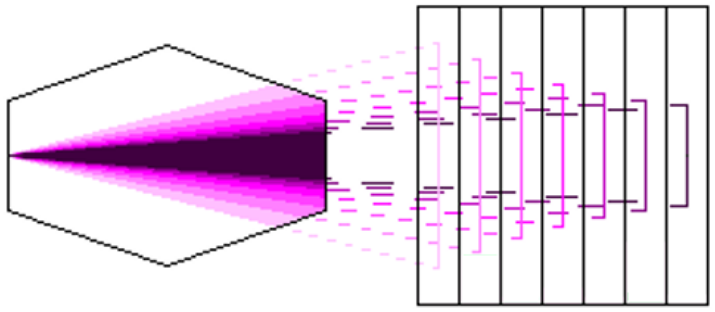

[1]Schulte et al. 2008 *Med. Phys.* [2]Collins-Fekete et al. 2015 *Phys. Med. Biol.* [3]Lazos et al. *2021 Phys. Med. Biol.*

Maximum Likely Path in list-mode detector configuration

- The list-mode detector configuration provides:
  - Position t and angle θ (vector y) at the entrance and exit of the object of interest (y_0 and y_2)

$$\hookrightarrow \; y = \begin{pmatrix} t \\ \theta \end{pmatrix}$$

  - WET of the single ion (proton)
- The Bayesian terminology defines:
  - $L(y_1|y_0)$ prior likelihood, find y_1 in u_1 given y_0 in u_0
  - $L(y_2|y_1)$ likelihood, find y_2 in u_2 given y_1 in u_1
  - $L(y_1|y_2)$ posterior likelihood, find y_1 in u_1 given y_2 in u_2

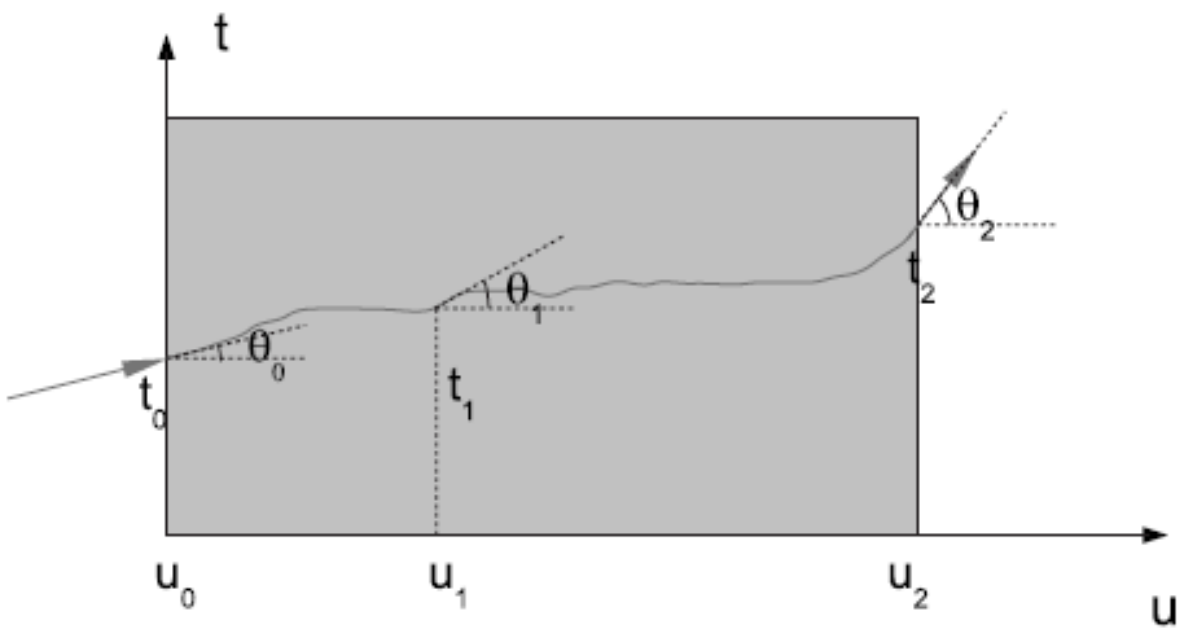

Schulte, R. W., Penfold, S. N., Tafas, J. T., & Schubert, K. E. (2008). A maximum likelihood proton path formalism for application in proton computed tomography. Medical physics, 35(11), 4849-4856.

Maximum Likely Path in list-mode detector configuration

- Relying on the Bayesian theorem, the maximum likely path (MLP) is defined as $y_1 = y_{MLP}$ maximizing the posterior likelihood

$$\underbrace{P(A|B)}_{\text{posterior}} = \underbrace{P(A)}_{\text{prior}} \times \frac{\overbrace{P(B|A)}^{\text{likelihood}}}{\underbrace{P(B)}_{\text{marginal}}}$$

https://www.freecodecamp.org/news/bayes-rule-explained/
https://seeve.medium.com/machine-learning-bayes-theorem-2f48c33d51e5

$$P(\mathrm{A}|\mathrm{B}) = \frac{P(\mathrm{B}|A) \cdot P(A)}{P(B)}$$

Probability of B occurring given evidence A has already occurred

Probability of A occurring

Probability of A occurring given evidence B has already occurred

Probability of B occurring

$$L(y_1|y_2) = L(y_2|y_1)L(y_1|y_0) \quad \Rightarrow \quad \begin{pmatrix} \partial t_1 \\ \partial \theta_1 \end{pmatrix} L(y_1|y_2) = \begin{pmatrix} 0 \\ 0 \end{pmatrix}$$

Bayesian theorem

Posterior likelihood maximization

Maximum Likely Path in list-mode detector configuration

- According to the Fermi-Eyges theory of Multiple Coulomb Scattering (MCS) the probability density function of the prior likelihood can be described as a bivariate Gaussian

$$L(y_1|y_0) = \exp(-\frac{1}{2} y_1^T \Sigma_1^{-1} y_1) \quad \text{with} \quad \Sigma_1 = \begin{pmatrix} \sigma_{t_1}^2 & \sigma_{t_1\theta_1}^2 \\ \sigma_{t_1\theta_1}^2 & \sigma_{\theta_1}^2 \end{pmatrix}$$

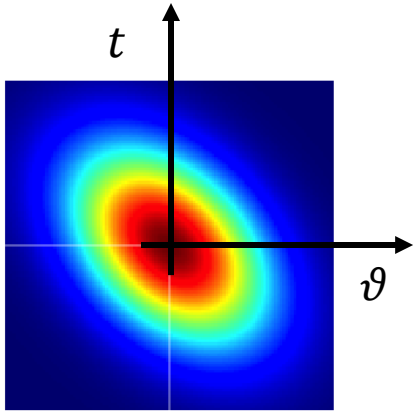

variance and covariance of t_1 and θ_1,
referred to as scattering matrix

Maximum Likely Path in list-mode detector configuration

- The coordinate system is changed according to position and angle in u_1 by means of a roto-translation

$$y_1' = y_1 - R_0 y_0 \quad \text{where} \quad R_0 = \begin{pmatrix} 1 & u_1 - u_0 \\ 0 & 1 \end{pmatrix}$$

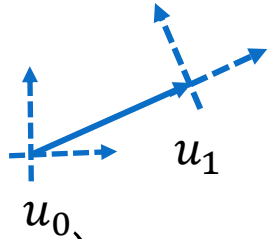

  - The prior likelihood becomes:

$$L(y_1|y_0) = \exp\left(-\frac{1}{2}(y_1^T - y_0^T R_0^T)\Sigma_1^{-1}(y_1 - R_0 y_0)\right)$$

  - Similarly, the likelihood is expressed as

$$L(y_2|y_1) = \exp\left(-\frac{1}{2}(y_2^T - y_1^T R_1^T)\Sigma_2^{-1}(y_2 - R_1 y_1)\right)$$

with $y_2' = y_2 - R_1 y_1$ where $R_1 = \begin{pmatrix} 1 & u_2 - u_1 \\ 0 & 1 \end{pmatrix}$

and with $\Sigma_2 = \begin{pmatrix} \sigma_{t_2}^2 & \sigma_{t_2\theta_2}^2 \\ \sigma_{t_2\theta_2}^2 & \sigma_{\theta_2}^2 \end{pmatrix}$ ⇨ variance and covariance of t_2 and θ_2, referred to as scattering matrix

Maximum Likely Path in list-mode detector configuration

- The posterior likelihood is then calculated according to the Bayesian theorem

$$L(y_1|y_2) = \exp\left(-\frac{1}{2}(y_1^T - y_0^T R_0^T)\Sigma_1^{-1}(y_1 - R_0 y_0) + \frac{1}{2}(y_2^T - y_1^T R_1^T)\Sigma_2^{-1}(y_2 - R_1 y_1)\right) = \exp(-\chi^2)$$

$$y = e^{f(x)}$$
$$y' = e^{f(x)} f'(x)$$

$$y' = 0 \rightarrow f'(x) = 0$$

$$\chi^2 = \frac{1}{2}((y_1^T\Sigma_1^{-1}y_1 - 2y_0^T R_0^T\Sigma_1^{-1}y_1 + y_0^T R_0^T\Sigma_1^{-1}R_0 y_0 + y_2^T\Sigma_2^{-1}y_2 - 2y_1^T R_1^T\Sigma_2^{-1}y_2 + y_1^T R_1^T\Sigma_2^{-1}R_1 y_1)$$

$$\nabla\chi^2 = (\Sigma_1^{-1} + R_1^T\Sigma_2^{-1}R_1)y_1 - \Sigma_1^{-1}R_0 y_0 - R_1^T\Sigma_2^{-1}y_2)$$

$$y_{MLP} = (\Sigma_1^{-1} + R_1^T\Sigma_2^{-1}R_1)^{-1}(\Sigma_1^{-1}R_0 y_0 + R_1^T\Sigma_2^{-1}y_2)$$

- Given position and angle at the entrance and the exit of the object of interest, and relying on probability density function of the MCS (Fermi-Eyges theory), an estimation of the ion (proton) trajectory is obtained

Fermi-Eyges theory for MCS

$$\begin{cases} \sigma_{t_1}^2(u_0,u_1) = E_0^2\left(1+0.038\ln\left(\frac{u_1-u_0}{X_{H_2O}}\right)\right)^2 \int_{u_0}^{u_1} \frac{(u_1-u)^2}{X_{H_2O}\beta^2(u)p^2(u)}\,du \\ \sigma_{\theta_1}^2(u_0,u_1) = E_0^2\left(1+0.038\ln\left(\frac{u_1-u_0}{X_{H_2O}}\right)\right)^2 \int_{u_0}^{u_1} \frac{1}{X_{H_2O}\beta^2(u)p^2(u)}\,du \\ \sigma_{t_1\theta_1}^2(u_0,u_1) = E_0^2\left(1+0.038\ln\left(\frac{u_1-u_0}{X_{H_2O}}\right)\right)^2 \int_{u_0}^{u_1} \frac{(u_1-u)}{X_{H_2O}\beta^2(u)p^2(u)}\,du \end{cases}$$

$$\begin{cases} \sigma_{t_2}^2(u_1,u_2) = E_0^2\left(1+0.038\ln\left(\frac{u_2-u_1}{X_{H_2O}}\right)\right)^2 \int_{u_1}^{u_2} \frac{(u_2-u)^2}{X_{H_2O}\beta^2(u)p^2(u)}\,du \\ \sigma_{\theta_2}^2(u_1,u_2) = E_0^2\left(1+0.038\ln\left(\frac{u_2-u_1}{X_{H_2O}}\right)\right)^2 \int_{u_1}^{u_2} \frac{1}{X_{H_2O}\beta^2(u)p^2(u)}\,du \\ \sigma_{t_2\theta_2}^2(u_1,u_2) = E_0^2\left(1+0.038\ln\left(\frac{u_2-u_1}{X_{H_2O}}\right)\right)^2 \int_{u_1}^{u_2} \frac{(u_2-u)}{X_{H_2O}\beta^2(u)p^2(u)}\,du \end{cases}$$

$$\Rightarrow \quad \Sigma_1 = \begin{pmatrix} \sigma_{t_1}^2 & \sigma_{t_1\theta_1}^2 \\ \sigma_{t_1\theta_1}^2 & \sigma_{\theta_1}^2 \end{pmatrix} \qquad \Sigma_2 = \begin{pmatrix} \sigma_{t_2}^2 & \sigma_{t_2\theta_2}^2 \\ \sigma_{t_2\theta_2}^2 & \sigma_{\theta_2}^2 \end{pmatrix}$$

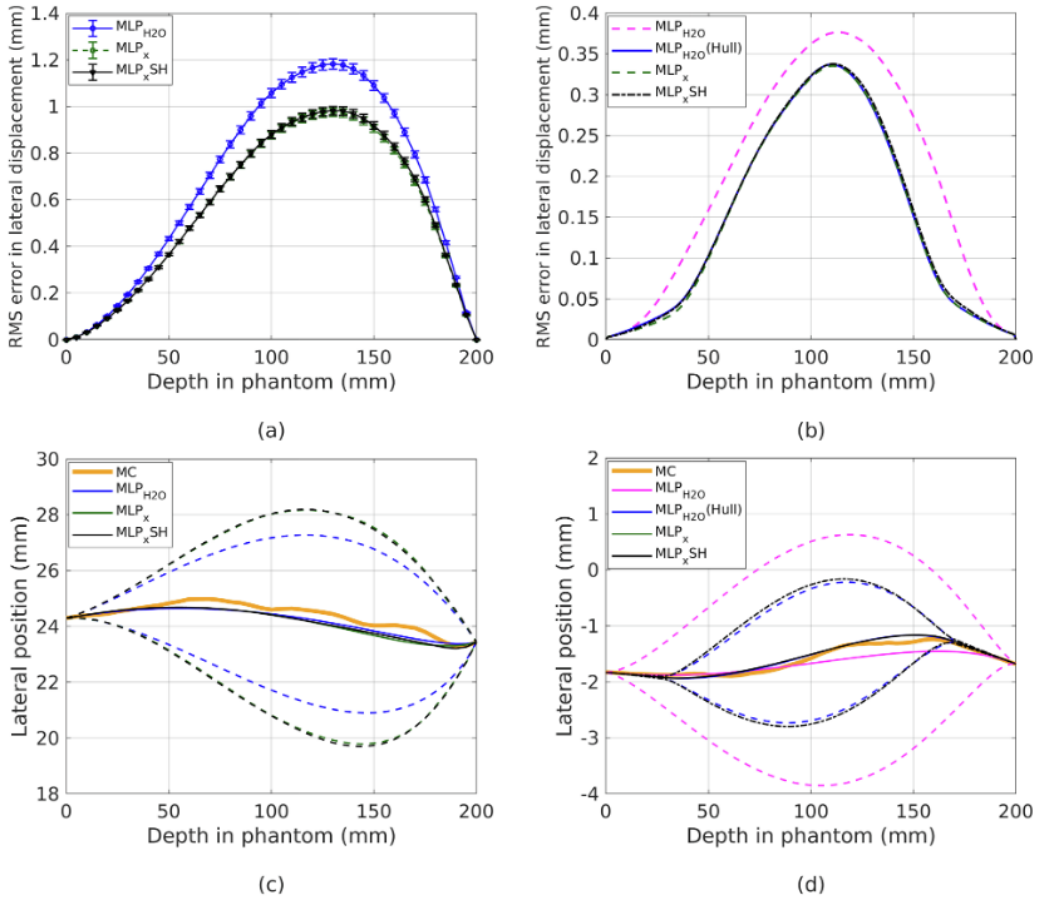

Brooke, M. D., & Penfold, S. N. (2020). An inhomogeneous most likely path formalism for proton computed tomography. Physica Medica, 70, 184-195.

Outlook

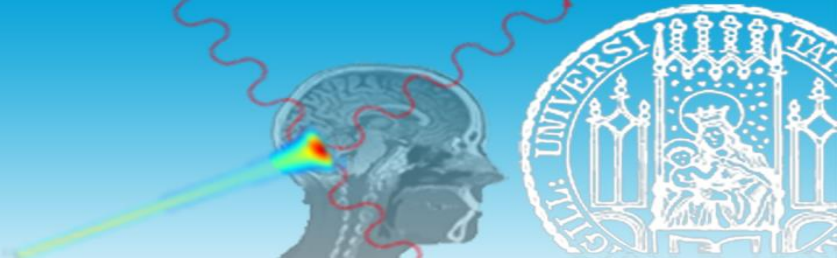

- Ion imaging is emerging in the research context of ion beam therapy
- Proton imaging is currently dominating in literature because of the availability of the ion source in ion beam therapy facilities worldwide
  - The first prototypes for proton imaging have been realized according to list-mode detector configuration
  - Integration-mode detector configuration has been investigated mostly for range verification in carbon ion therapy
- However, the interest for integration-mode detector configuration is now growing also for proton imaging
- Clinical translation from X-ray imaging to ion imaging is likely foreseen based on a limited number of ion radiographies (due to geometrical and dosimetric constraints) acquired with integration-mode detector configuration and combined with X-ray imaging, as currently available for treatment planning

Methodological challenges

Outlook

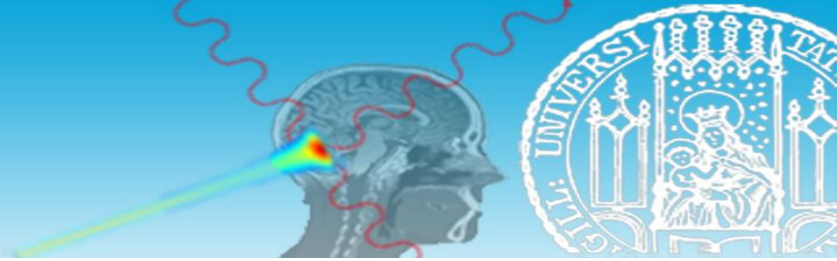

- Relying on recent hardware and software developments, ion imaging could potentially match the imaging requirements for clinical applications in ion beam therapy
- However, no detector has been so far integrated into a treatment room
- Ion imaging experiments currently suffer from important geometrical limitations, long acquisition time and high imaging dose
- As most of the ion beam therapy facilities are not provided by rotating beam gantries and the most of the prototypes are based on bulky detectors, ion tomography experiments are currently performed by rotating the object of interest while keeping the detector aligned to the fixed beam nozzle
- Except for seated treatment positions which could be considered for ocular and cranial tumors, ion imaging would be impossible for most of the patients positioned on beds
- A game changer of a prompt clinical translation of ion imaging would be the integration of a movable imaging system (i.e., mounted on a robot) inside the treatment room

Technological challenges

Historical overview

- The very first experiment of proton radiography was demonstrated in the 1960s based on a photographic film[1], followed by the first proton tomography in 1970s based on sodium iodide (NaI) scintillation counters[2]

- The pioneer prototype provided with tracking detector was proposed by Hanson *et al*. at the Los Alamos Laboratory in the late 1970s and early 1980s[3]
  - Tracking detector: one multi-wire proportional chamber to track *exit* position
  - Range detector: hyperpure germanium calorimeter for residual energy measurement (earlier experiments) and a stack of plastic scintillators for proton range measurement (later experiments)

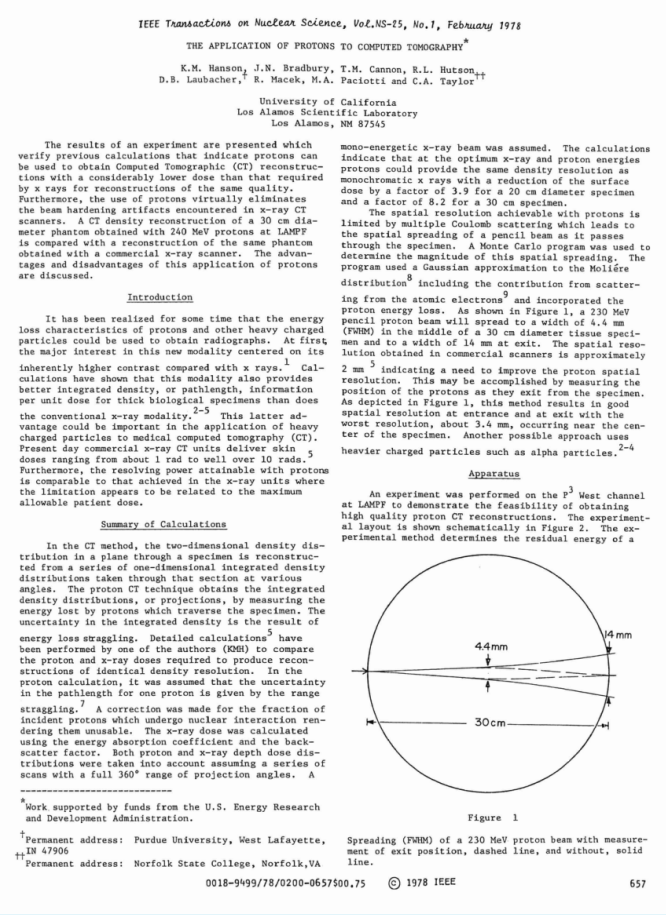

IEEE Transactions on Nuclear Science, Vol.NS-25, No.1, February 1978

THE APPLICATION OF PROTONS TO COMPUTED TOMOGRAPHY*

K.M. Hanson, J.N. Bradbury, T.M. Cannon, R.L. Hutson, D.B. Laubacher,† R. Macek, M.A. Paciotti and C.A. Taylor††

University of California
Los Alamos Scientific Laboratory
Los Alamos, NM 87545

The results of an experiment are presented which verify previous calculations that indicate protons can be used to obtain Computed Tomographic (CT) reconstructions with a considerably lower dose than that required by x rays for reconstructions of the same quality. Furthermore, the use of protons virtually eliminates the beam hardening artifacts encountered in x-ray CT scanners. A CT density reconstruction of a 30 cm diameter phantom obtained with 240 MeV protons at LAMPF is compared with a reconstruction of the same phantom obtained with a commercial x-ray scanner. The advantages and disadvantages of this application of protons are discussed.

Introduction

It has been realized for some time that the energy loss characteristics of protons and other heavy charged particles could be used to obtain radiographs. At first, the major interest in this new modality centered on its inherently higher contrast compared with x rays.[1] Calculations have shown that this modality also provides better integrated density, or pathlength, information per unit dose for thick biological specimens than does the conventional x-ray modality.[2-5] This latter advantage could be important in the application of heavy charged particles to medical computed tomography (CT). Present day commercial x-ray CT units deliver skin doses ranging from about 1 rad to well over 10 rads.[5] Furthermore, the resolving power attainable with protons is comparable to that achieved in the x-ray units where the limitation appears to be related to the maximum allowable patient dose.

Summary of Calculations

In the CT method, the two-dimensional density distribution in a plane through a specimen is reconstructed from a series of one-dimensional integrated density distributions taken through that section at various angles. The proton CT technique obtains the integrated density distributions, or projections, by measuring the energy lost by protons which traverse the specimen. The uncertainty in the integrated density is the result of energy loss straggling. Detailed calculations[5] have been performed by one of the authors (KMH) to compare the proton and x-ray doses required to produce reconstructions of identical density resolution. In the proton calculation, it was assumed that the uncertainty in the pathlength for one proton is given by the range straggling.[7] A correction was made for the fraction of incident protons which undergo nuclear interaction rendering them unusable. The x-ray dose was calculated using the energy absorption coefficient and the backscatter factor. Both proton and x-ray depth dose distributions were taken into account assuming a series of scans with a full 360° range of projection angles. A mono-energetic x-ray beam was assumed. The calculations indicate that at the optimum x-ray and proton energies protons could provide the same density resolution as monochromatic x rays with a reduction of the surface dose by a factor of 3.9 for a 20 cm diameter specimen and a factor of 8.2 for a 30 cm specimen.

The spatial resolution achievable with protons is limited by multiple Coulomb scattering which leads to the spatial spreading of a pencil beam as it passes through the specimen. A Monte Carlo program was used to determine the magnitude of this spatial spreading. The program used a Gaussian approximation to the Molière distribution[8] including the contribution from scattering from the atomic electrons[9] and incorporated the proton energy loss. As shown in Figure 1, a 230 MeV pencil proton beam will spread to a width of 4.4 mm (FWHM) in the middle of a 30 cm diameter tissue specimen and to a width of 14 mm at exit. The spatial resolution obtained in commercial scanners is approximately 2 mm [5] indicating a need to improve the proton spatial resolution. This may be accomplished by measuring the position of the protons as they exit from the specimen. As depicted in Figure 1, this method results in good spatial resolution at entrance and at exit with the worst resolution, about 3.4 mm, occurring near the center of the specimen. Another possible approach uses heavier charged particles such as alpha particles.[2-4]

Apparatus

An experiment was performed on the P[3] West channel at LAMPF to demonstrate the feasibility of obtaining high quality proton CT reconstructions. The experimental layout is shown schematically in Figure 2. The experimental method determines the residual energy of a

Figure 1

Spreading (FWHM) of a 230 MeV proton beam with measurement of exit position, dashed line, and without, solid line.

*Work supported by funds from the U.S. Energy Research and Development Administration.

†Permanent address: Purdue University, West Lafayette, IN 47906
††Permanent address: Norfolk State College, Norfolk, VA

0018-9499/78/0200-0657$00.75

[1] Koehler 1968 *Science*
[2] Cormack and Koehler 1976 *Phys. Med. Biol.*
[3] Hanson et al. 1978 *IEEE Trans. Nucl. Sci.*

Historical overview

- The modern era of ion imaging was initiated by the two systems developed at the Paul Scherrer Institute (PSI) from the mid 1990s[1a]

- The first system was inspired by the pioneer prototype from Hanson *et al*.

  - Tracking detector: two multi-wire proportional chambers based on gas ionization (avalanche) in high electric field to track *entrance* and *exit* positions of the proton

  - Range detector: a plastic scintillation counter (trigger) coupled with a sodium iodide (NaI) crystals detector (calorimeter)

    - Proton rate of ~ 1 kHz

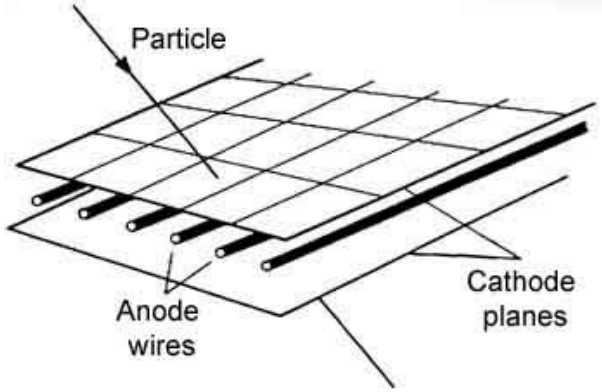

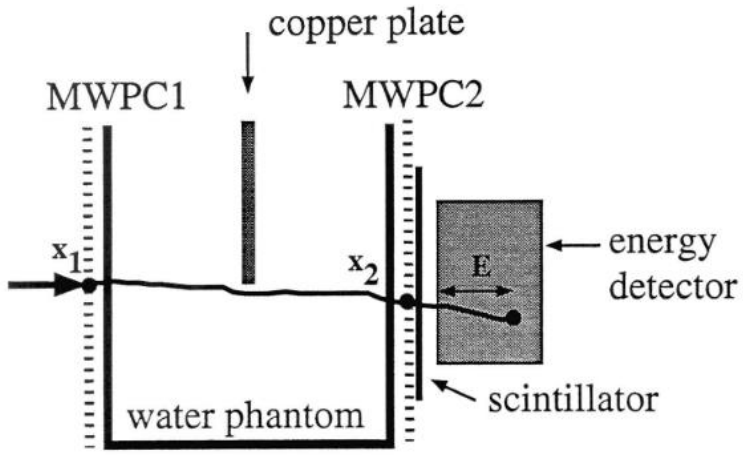

[1a]Schneider and Pedroni 1995 *Med. Phys.*

Historical overview

- The second system was based on plastic scintillators read out by photomultipliers[1b]
  - Tracking detector: two plastic scintillating fibre *hodoscope* (from the Greek “hodos” - path and “skopos” - observe)
  - Range detector: a range *telescope* (from the Greek “tele” - far and “skopos” - observe) based on a stack of closely packed and optically isolated plastic scintillator tiles
    - Proton rate of ~ 1 MHz

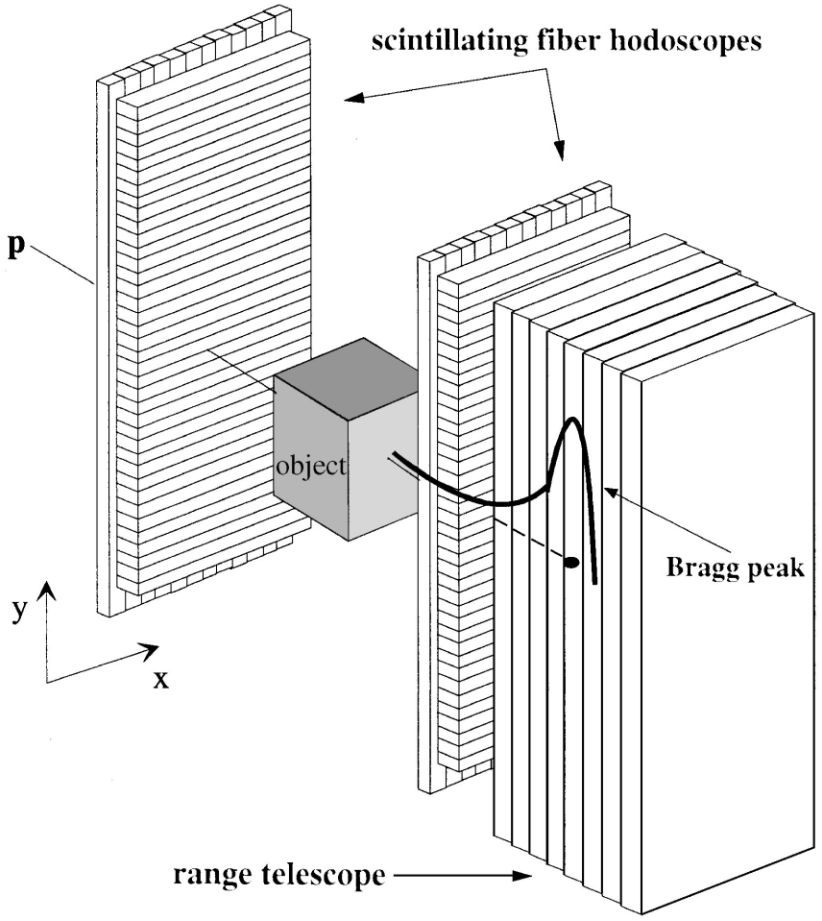

[1b] Pemler et al. 1999 *Nucl. Instrum. Methods Phys. Res. A*

Historical overview

- Started in 2003, a collaboration within Loma Linda University (LLU), University of California Santa Cruz (UCSC) and Northern Illinois University (NIU) developed a prototype system and published literature milestones in proton imaging
  - Tracking detector: four silicon strip detectors (proton rate of ~25 MHz) to track *entrance* and *exit* position and direction of the proton
  - First range detector: CsI:Tl (Thallium doped Cesium Iodide) crystal detector (calorimeter) paired to silicon photodiodes (semiconductor p–n junctions that convert light into an electrical current)[1]
  - Second range detector: stack of fast plastic scintillators read out by photomultiplier tubes[2]

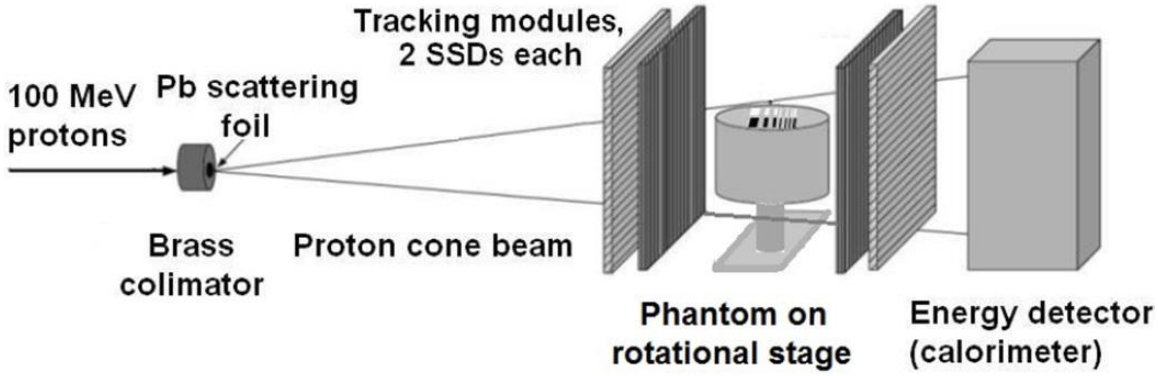

[1]Sadrozinsky et al. 2004 *IEEE Trans. Nucl. Sci.*
[2]Bashkirov et al. 2016 *Nucl. Instrum. Methods Phys. Res. A*

Historical overview

- A pioneering prototype of a range telescope (multiple layers, single energy) for pencil beams was realized at the *Helmholtzzentrum für Schwerionenforschung* (GSI) and investigated as range verification technique at the Heidelberg Ion Beam Therapy Center (HIT) in collaboration with researchers from the Heidelberg University Hospital

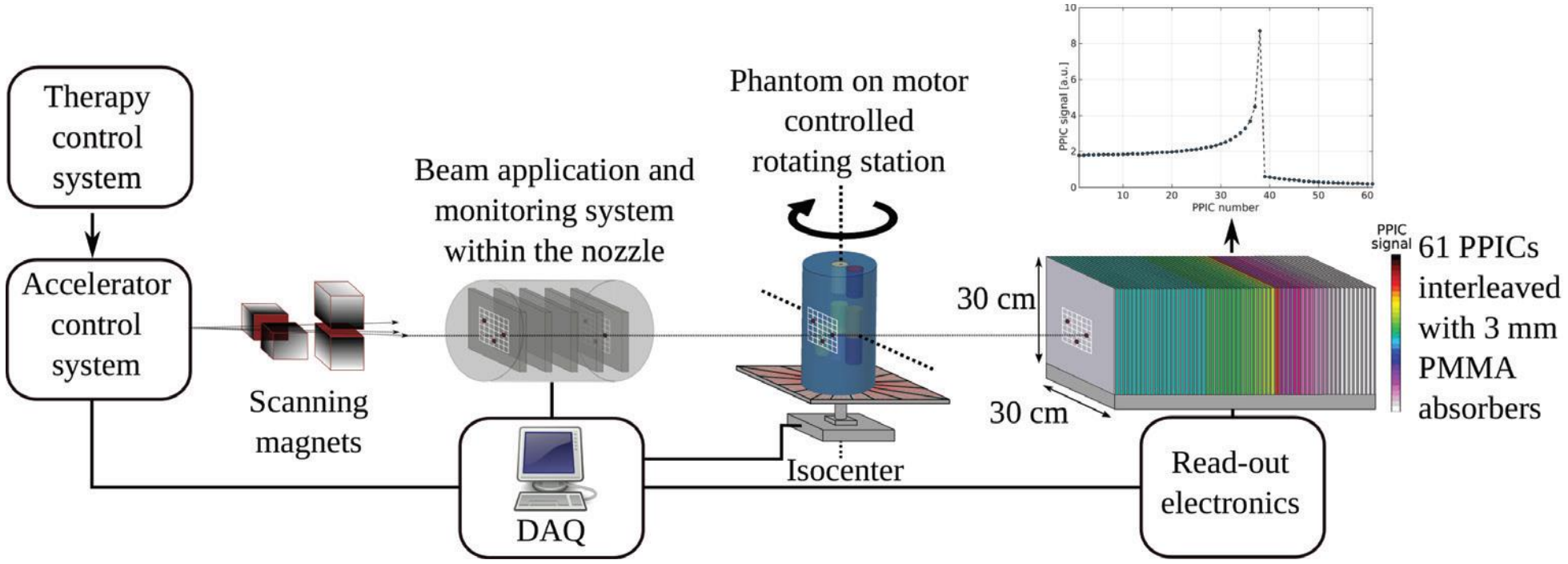

Rinaldi et al. 2013 *Phys. Med. Biol.*
Meyer, Gianoli, … et al. 2017 *Phys. Med. Biol.*

Historical overview

- Pixelated (commercial) silicon detectors (single layer, multiple energies) based on active variation of the energy of the pencil beams[1] or based on range modulator wheel in passive beams[2] or based on poly-energetic laser-driven accelerated beams[3]

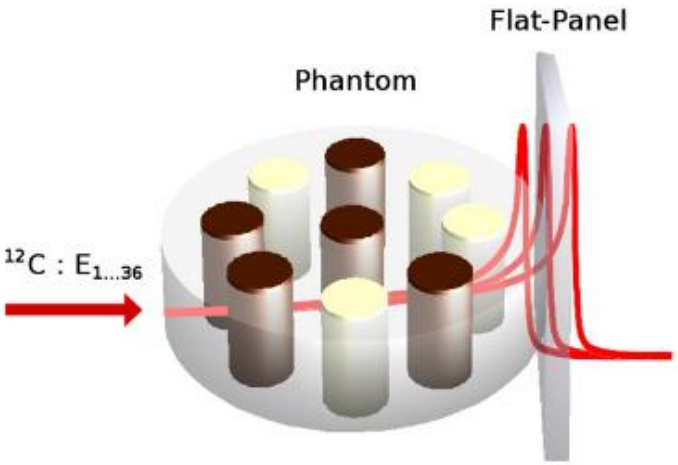

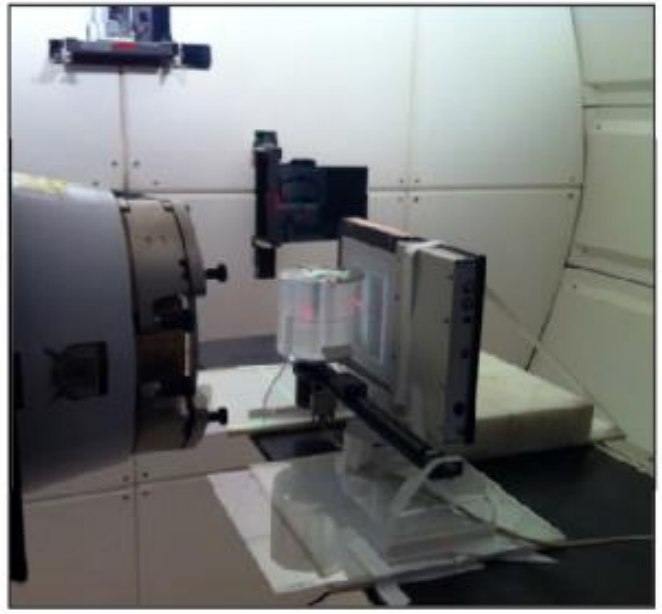

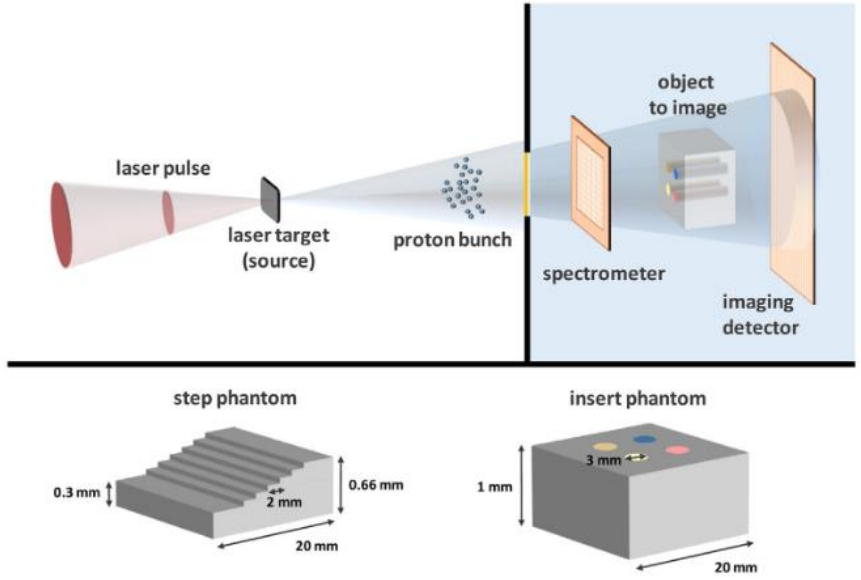

[1]Telsemeyer et al. 2012 *Phys. Med. Biol.*

[2]Testa et al. 2013 *Phys. Med. Biol.*

[3]Würl, Gianoli, … et al. 2020 *Z. fur Med. Phys.*